Since January 2020 Elsevier has created a COVID-19 resource centre with free information in English and Mandarin on the novel coronavirus COVID-19. The COVID-19 resource centre is hosted on Elsevier Connect, the company's public news and information website.

EGCG as an anti-SARS-CoV-2 agent: Preventive *versus* therapeutic potential against original and mutant virus

Vladimir Tsvetkov [a, b, c, 1], Anna Varizhuk [a, d, e, 1], Liubov Kozlovskaya [f, g, 1], Anna Shtro [h], Olga Lebedeva [a, d], Andrey Komissarov [h], Tatjana Vedekhina [a], Valentin Manuvera [a, d, e], Olga Zubkova [a], Artem Eremeev [a, d], Elena Shustova [f], Galina Pozmogova [a], Dmitry Lioznov [h], Aydar Ishmukhametov [f, g], Vassili Lazarev [a, d, e, *], Maria Lagarkova [a, d, **]

[a] Federal Research and Clinical Center of Physical Chemical Medicine of Federal Medical Biological Agency, Malaya Pirogovskaya str. 1a, 119435, Moscow, Russia
[b] World-Class Research Center "Digital Biodesign and Personalized Healthcare", I.M. Sechenov First Moscow State Medical University, Trubetskaya Str. 8-2, 119991, Moscow, Russia
[c] A.V. Topchiev Institute of Petrochemical Synthesis RAS, Moscow, 119071, Russia
[d] Center for Precision Genome Editing and Genetic Technologies for Biomedicine, Federal Research and Clinical Center of Physical-Chemical Medicine of Federal Medical Biological Agency, 119435, Moscow, Russia
[e] Moscow Institute of Physics and Technology, Institutskiy Pereulok 9, Dolgoprudny, 141701, Russia
[f] Chumakov Federal Scientific Center for Research and Development of Immune-and-Biological Products of Russian Academy of Sciences, Poselok Instituta Poliomiyelita 8, 108819, Moscow, Russia
[g] Institute of Translational Medicine and Biotechnology, Sechenov Moscow State Medical University, Nakhimovsky av. 45, 117418, Moscow, Russia
[h] Smorodintsev Research Institute of Influenza, Professora Popova str., 15/17, 197376, Sankt-Peterburg, Russia

ARTICLE INFO

ABSTRACT

In the search for anti-SARS-CoV-2 drugs, much attention is given to safe and widely available native compounds. The green tea component epigallocatechin 3 gallate (EGCG) is particularly promising because it reportedly inhibits viral replication and viral entry *in vitro*. However, conclusive evidence for its predominant activity is needed. We tested EGCG effects on the native virus isolated from COVID-19 patients in two independent series of experiments using VERO cells and two different treatment schemes in each series. The results confirmed modest cytotoxicity of EGCG and its substantial antiviral activity. The preincubation scheme aimed at infection prevention has proven particularly beneficial. We complemented that finding with a detailed investigation of EGCG interactions with viral S-protein subunits, including S2, RBD, and the RBD mutant harboring the N501Y mutation. Molecular modeling experiments revealed N501Y-specific stacking interactions in the RBD-ACE2 complex and provided insight into EGCG interference with the complex formation. Together, these findings provide a molecular basis for the observed EGCG effects and reinforce its prospects in COVID-19 prevention therapy.

© 2021 Elsevier B.V. and Société Française de Biochimie et Biologie Moléculaire (SFBBM). All rights reserved.

1. Introduction

Prevention and treatment of COVID-19 is of utmost importance. In the search for new antiviral agents, particular attention is paid to native compounds due to their availability and safety. Epigallocatechin-3-gallat (EGCG, Fig. 1A), a major component of the green tea extract, is currently in the limelight, as it shows pronounced inhibitory activity against various types of viruses, especially with positive-sense single-stranded RNA genomes [1]. Discussions on EGCG applicability for SARS-CoV-2 treatment or prevention are mostly grounded by the results of lentiviral system-based assays [2]. Direct evidence for EGCG activity against SARS-CoV-2 is limited [3], and detailed experiments with the live virus and various treatment schemes are much needed.

* Corresponding author. Malaya Pirogovaskaya str. 1A, Moscow, 119435, Russia.
** Corresponding author. Malaya Pirogovaskaya str. 1A, Moscow, 119435, Russia.
E-mail addresses: lazarev@rcpcm.org (V. Lazarev), lagar@rcpcm.org (M. Lagarkova).
[1] These authors contributed equally.
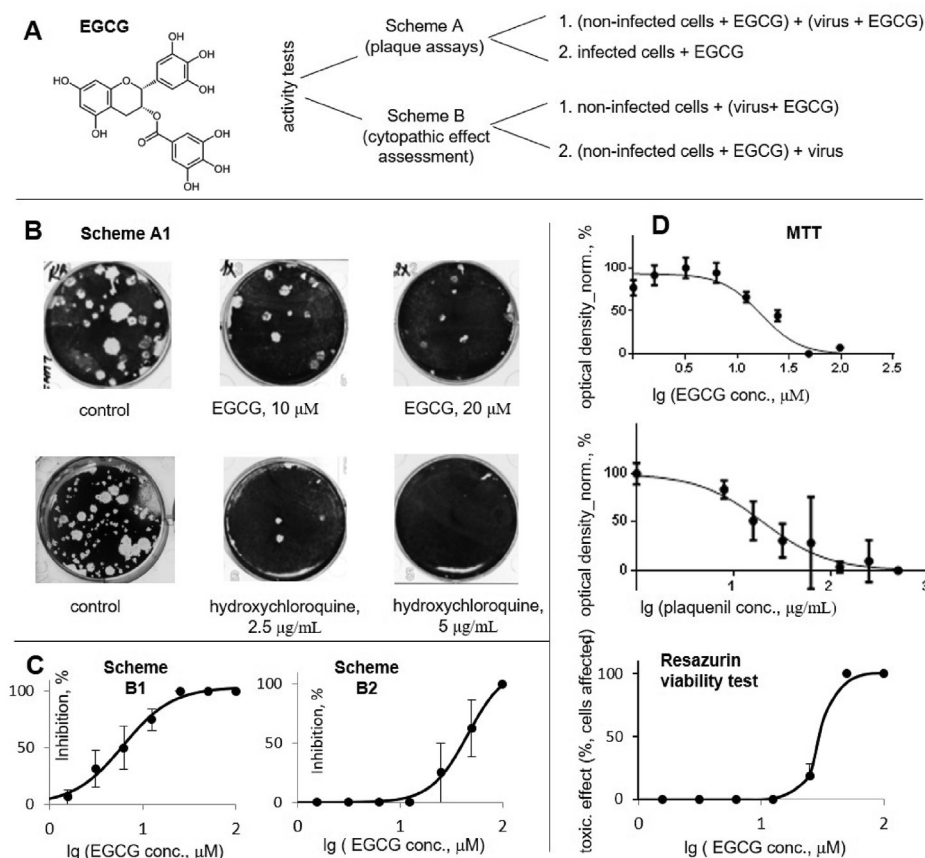
Fig. 1. Antiviral activity of EGCG. (A) Summary of the experimental schemes. (B) Representative plaque images obtained in scheme-A experiments. (C) Inhibition curves, scheme B1. (D) Results of the cell viability assays.

2. Materials and methods

2.1. Virus, cells, and cell viability assays

EGCG was purchased from Fisher Scientific (USA), hydroxychloroquine was obtained from Sigma Aldrich (USA), and β-d-N^4-Hydroxycytidine (NHC) was purchased from Cell Signaling (USA). Vero cell line was obtained from Biologicals, World Health Organization, Switzerland. Cells were maintained in Dulbecco's Modified Eagle Medium (DMEM, FSBSI "Chumakov FSC R&D IBP RAS", Russia), supplemented with fetal bovine serum (FBS, Gibco, 5%), streptomycin (0.1 mg/ml), and penicillin (100 units/ml) (PanEco, Russia). The SARS-CoV-2 strain PIK35 (GISAID EPI_ISL_428852) was isolated from a nasopharyngeal swab sample of a COVID-19 patient [18]. The virus was passaged 5 times in Vero cells and was stored as infected cells suspension at -70 °C. The effects of EGCG, NHC and hydroxychloroquine on cell metabolic activity and viability were assessed using standard MTT and resazurin tests (for more details, see supplementary text box S1).

2.2. SARS-CoV-2 inhibition test

2.2.1. Scheme A1

Two-fold dilutions of EGCG or hydroxychloroquine were added to a confluent monolayer of non-infected Vero cells in 6-well plates prior to the infection. After 2 h incubation at 37 °C (5% CO_2), virus-EGCG or virus-hydroxychloroquine mixes were added, and the cells were incubated for additional 2 h at 37 °C (5% CO_2). Then, the virus and EGCG or hydroxychloroquine were removed, and the cells were incubated at 37 °C for 3 days under a solid overlay containing 0.9% agarose. At the final stage, the cells were fixed and stained with a 0.2% solution of crystal violet in 50% ethanol containing 0.05% glutaric aldehyde.

2.2.2. Scheme A2

The cells were infected with virus and incubated for 2 h incubation at 37 °C (5% CO2). Then, virus was removed, and a 0.9% agarose overlay containing the EGCG or hydroxychloroquine was applied. The cells were incubated at 37 °C for 3 days under the overlay, and then fixed and stained. To obtain inhibition curves, the percentage of plaques in EGCG/hydroxychloroquine-treated wells relative to the control well was calculated for each concentration.

2.2.3. Scheme B1

Two-fold dilutions of EGCG or NHC were prepared in DMEM (FSBSI "Chumakov FSC R&D IBP RAS", Russia). These solutions were mixed with equal volumes of the virus suspension containing $50-200$ $CCID_{50}$ per well. After 1 h incubation at 37 °C, virus-EGCG or virus-NHC mixes were added to the confluent Vero cell monolayers in 2 replicates. After a 5-day incubation at 37 °C, cytopathic effect (CPE) was visually accessed via microscope. EC_{50} values were calculated according to the Karber method [19].

2.2.4. Scheme B2

EGCG or NHC solutions in DMEM were added to the confluent Vero cell monolayers and incubated for 24 h. Then, virus suspension containing $50-200$ $CCID_{50}$ per well was added. After a 5-day incubation at 37 °C, CPE was assessed visually.

2.3. Recombinant proteins

To obtain the recombinant receptor-binding domain (RBD) of protein S in human cell culture, the pcDNA-RBD plasmid was constructed based on the pcDNA-3.4 plasmid (Thermo Fisher Scientific, USA). The RBD-coding DNA fragment was obtained by PCR amplification of SARS-CoV-2 cDNA. The recombinant gene in the pcDNA-RBD plasmid encoded RBD with a signal peptide and a C-terminal 6His-Tag. To produce human RBD-producing cells, Expi293F cells (ThermoFisher Scientific, USA) were transfected with the pcDNA-RBD plasmid using the Expi293 Expression System Kit (ThermoFisher Scientific, USA). After transfection, the cells were cultivated for 72 h in 5% CO_2 at 37 °C upon stirring at 125 rpm. Next, the cells were precipitated by centrifugation and the protein was isolated from culture medium by metal chelate chromatography using a Ni Sepharose High sorbent Performance (GE Healthcare, USA).

The N501Y mutant of RBD (RBDm) and S2 protein were obtained analogously to RBD.

2.4. Binding assays and circular dichroism spectroscopy

For *in vitro* binding assays, SARS-CoV-2 recombinant proteins RBD, its N501Y mutant RBDm, and S2 were labeled using the NT™ Protein Labeling Kit RED-NHS (Nanotemper, Germany) and mixed with increasing concentrations of EGCG in a 10 mM potassium-phosphate buffer, pH 7.4, supplemented with 0.05% Tween-20. The final protein concentration was 50 nM. The protein-ligand mixtures were stored at room temperature for 15 min prior to all measurements.

MST curves were registered using Monolith NT.115, equipped with a RED/GREEN detector, and standard capillaries (NanoTemper, Germany) at 22 °C. The dependence of the normalized fluorescence immediately after T-jump (1.5 s MST time) on EGCG concentration was analyzed using MO.Affinity Analysis software (NanoTemper, Germany). Integral normalized fluorescence and the bleaching rate of the label in EGCG-protein mixtures were registered in parallel to MTS and analyzed using MO.Affinity Analysis software. Experimental data were fitted to a Hill model.

To verify EGCG-induced conformational changes in RBD, circular dichroism (CD) spectra of the protein or its complex with EGCG in 10 mM potassium-phosphate buffer, pH 7.4, were registered using Chrascan spectrophotometer (Applied Photophysics, UK) at 20 °C.

2.5. Molecular modeling

Molecular modeling was performed to elucidate the EGCG-RBD interaction mode. EGCG was docked to RBD surface to identify the most likely binding sites. The contributions of electrostatic and Van der Waals interactions, as well solvation energy, to the binding energy were considered. Details on docking and molecular dynamics simulations are provided in supplementary text box S2.

The 3D model of EGCG was downloaded for Protein Data Bank (PDB ID: 4AWM) and optimized using molecular graphics software package Sybyl-X software (Certara, USA). Partial charges of the atoms were calculated according to the following scheme. Optimization and electron density distribution calculations were performed by using second-order Møller−Plesset perturbation theory (MP2) [20] and implicit consideration of the solvent effect with application of the conductor-like polarizable continuum model (CPCM) [21] and 6−31g* basis sets. Then Merz-Singh-Kollman scheme [22] was applied to obtained electron density distribution for calculation of grid for the electrostatic potential fitting with the following parameters: (6/41 = 10) - the number of surfaces around the atoms and (6/42 = 17) - the density of test points on these surfaces. The RESP (Restrained ElectroStatic Potential) method [23] was applied to fitting of the grid obtained in the previous step for calculation of partial atomic charges. All quantum mechanics simulations were carried out using Gaussian 09 program.

The model of RBD was downloaded from Protein Data Bank (PDB ID: 6VXX). For RBDm, N501 was substituted with Y501, and the model was reoptimized using molecular graphics software package Sybyl-X software (Certara, USA). The following settings were used: partial charges on the protein and parameters for interatomic interactions from Amber7ff02 force field, a non-bonded cut-off distance equal to 8 Å, the dielectric constant was equal 4.0, the number of iterations equal to 500, the simplex method in an initial optimization, and an energy gradient convergence criterion of 0.05 kcal/mol/Å.

3. Results and discussion

Here, we designed a series of experiments (schemes A1 and A2, Fig. 1A) to clarify whether EGCG is most efficient at preventing viral entry or replication. We evaluated EGCG effects on SARS-CoV-2-induced plaque and CPE formation using Vero cells and live viruses isolated from COVID-19 patients. In scheme A1, cells were first preincubated with EGCG for 2 h, and then treated with a virus-EGCG mixture. In scheme A2, cells were incubated with EGCG for 2 h after the infection. Plaque formation was analyzed 3 days after the infection (Fig. 1B). Hydroxychloroquine (hydroxychloroquine sulphate) was used as a positive control. Although Hydroxychloroquine efficiency *in vivo* is a controversial point [4,5], it has proven to inhibit SARS-CoV-2 *in vitro* [6]. The experiments were performed for a series of EGCG dilutions, and fitting of the resulting curves to the dose-response equation gave IC_{50} values of 4 ± 1 μM (scheme A1) and 10 ± 2 μM (scheme A2). This result indicates that inhibition of viral entry, rather than replication blockage, likely underlies EGCG activity. Moderate effects on viral replication are attributable to EGCG affinity for 3-chymotrypsin-like (3CL)-protease and/or RNA-dependent RNA polymerase of SARS-CoV-2. Both of these proteins have been predicted as EGCG targets based on docking experiments [7,8], and EGCG interaction with 3CL-protease binding has been confirmed *in vitro* [9].

The fact that EGCG is more potent at preventing SARS-CoV-2 entry than replication agrees with the previous reports of lenti-viral assays [2]. A growing body of data suggests that the preventive activity is due to EGCG interference with the interactions between SARS-CoV-2 and angiotensin converting enzyme 2 (ACE2) [2,7,8]. This is attributable to EGCG binding with spike (S) protein [10]. However, alternatives, such as EGCG interactions with the cell surface receptors or EGCG-induced alterations of membrane fluidity [11], have not been tested properly with the live virus.

To partially fill this gap, we designed another series of experiments (schemes B1 and B2, Fig. 2A) and evaluated the impact of EGCG on SARS-CoV-2-induced cytopathic effect (CPE). In scheme B1, the virus was preincubated with EGCG for 1 h, and then added to Vero cells. In scheme B2, the cells were preincubated with EGCG for 1 h and then the virus was added. A known broad-spectrum antiviral agent β-d-N^4-Hydroxycytidine (NHC) [12] was used as a positive control. Microscopy-based analysis of the cytopathic effect was performed 5 days after the infection. The inhibition curves are shown in Fig. 1C. Scheme B1 was clearly superior to B2 (IC_{50} values of 5 ± 1 μM and >40 μM, respectively).

Cytotoxicity of EGCG toward Vero cells was assessed in both 'A' and 'B' series using MTT and resazurin viability tests, respectively (Fig. 1D). Additional cytotoxicity tests were performed using primary human fibroblasts (Fig. S1). The tests gave comparable CC_{50} values, which were 6−7 times higher than EC_{50} values obtained in Schemes A1 and B1. All EC_{50} and CC_{50} data are summarized in
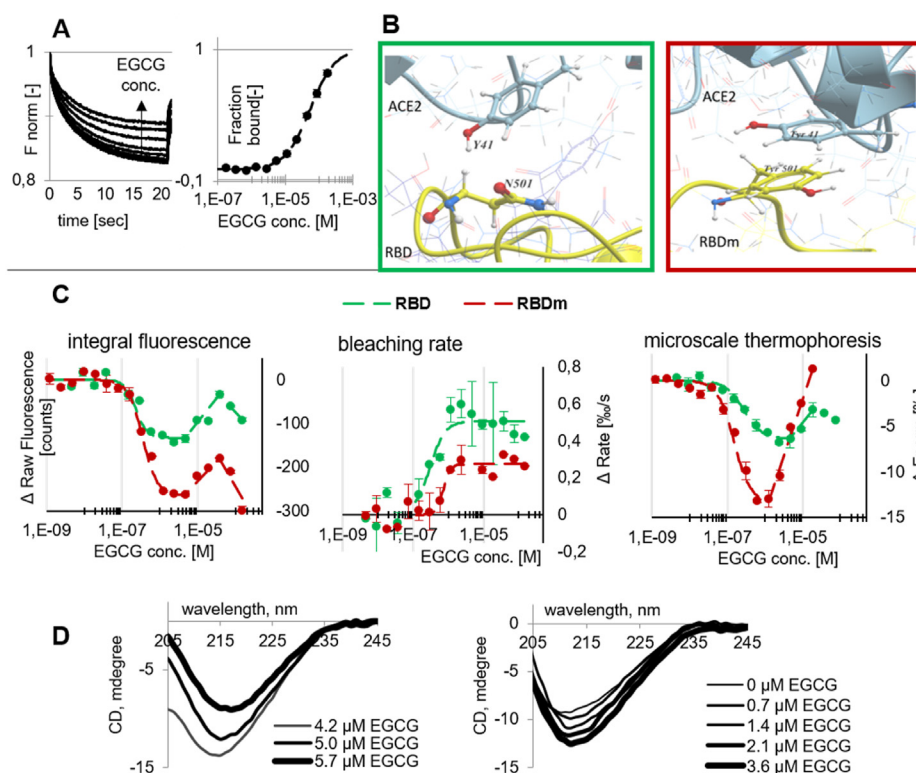
Fig. 2. Affinity of EGCG for SARS-CoV-2 proteins. (A) Interactions with S2: microscale thermophoresis kinetic curves (left) and the resulting binding curve (right). (B) Fragments of RBD and RBDm complexes with ACE2. (C) EGCG interactions with RBD and RBDm: binding curves obtained by monitoring fluorescence quenching, bleaching rate, and microscale thermophoresis. (D) Conformational changes in RBD upon interaction with EGCG evidenced by circular dichroism spectra.

Table 1
Cytotoxicity, inhibitory activity and selectivity index (SI) of EGCG compared to control drugs.

compound	scheme	CC50, μM	EC50, μM	SI
hydroxy-chloroquine	A1	39 ± 6	3 ± 1	13
	A2		7 ± 2	6
EGCG	A1	22 ± 6	4 ± 1	6
	A2		10 ± 2	2
	B1	33 ± 6	5 ± 1	7
	B2		43 ± 11	–
NHC	B1	>100	5.0 ± 0.6	>20
	B2		2.5 ± 0.7	>20

Table 1. Moderate cytotoxicity and minor anti-SARS-CoV-2 activity of EGCG upon preincubation with the cells (scheme B2) may arise from its effects on the cellular membrane (e.g., modulation of lipid rafts) [11,13]. The pronounced protective activity of EGCG upon preincubation with the virus (scheme B1) suggests that SARS-CoV-2 surface proteins, but not cellular proteins, are major targets of EGCG.

The two subunits of the entry-mediating virus surface spike protein (S1, which recognizes ACE2 receptor via its receptor binding domain, and S2, which mediates membrane fusion) have been considered previously as EGCG binding partners. Indirect assays argued against the decisive role of S2; while recombinant S1 showed affinity for EGCG in the micromolar concentration range [2]. Consistently with the data in the literature, we observed only weak EGCG binding with the fluorescently labeled S2 in microscale thermophoresis (MST)-based *in vitro* assays: Kd = 54 ± 6 μM (Fig. 2A), so we focused on the receptor binding domain of the S1 subunit (Fig. 2B).

We considered two variants of the receptor binding domain: the consensus one (RBD) and its analog harboring the N501Y mutation

in the ACE2-binding site (RBDm). The mutation concerned has been linked to increased transmissibility of B.1.1.7 ("UK variant") and several other circulating SARS-CoV-2 strains [14]. Reported molecular modeling and molecular dynamics (MD) simulations provided some insight into the observed effect of this mutation: it has been attributed to more efficient electrostatic interactions between RBDm and ACE2 [15] or hydrophobic interactions that predetermine positioning of RBDm Y501 residue between Y41 and K353 in hACE2 [16]. The latter variant agrees with the cryo-electron microscopy structure of the complex [17], but suggests only slightly increased RBDm binding affinity for ACE2 [16]. Our modeling results are also consistent with the published structures of the complex, but imply the possibility of stacking interactions between Y501 and Y41 residues, which explains substantially increased infectivity of the mutant (Fig. 2B).

We tested EGCG affinity for RBD and RBDm in MST assays using fluorescently labeled recombinant proteins and additionally monitored fluorescence quenching and bleaching rate (Fig. 2C). The results pointed to multistep/allosteric interactions: initial binding with Kd = 300 ± 200 nM (the major sigmoid part of the curve) was followed by a conformational rearrangement at low to medium micromolar concentrations. These findings were further confirmed by CD spectroscopy (Fig. 2D): the structured protein-specific CD band shifted from 210 to 215 nm upon titration with EGCG. Thus, EGCG binds RBD at submicromolar concentrations and modulates it conformation at micromolar concentrations, which may account for anti-SARS-CoV-2 activity of EGCG. To further elucidate EGCG-RBD interaction modes, molecular modeling experiments were performed.

To identify the most likely binding sites, EGCG was docked to RBD and RBDm surfaces. Two best conformations of the complexes obtained by docking (EGCG bound to sites 1 and 2, both at the RBD/
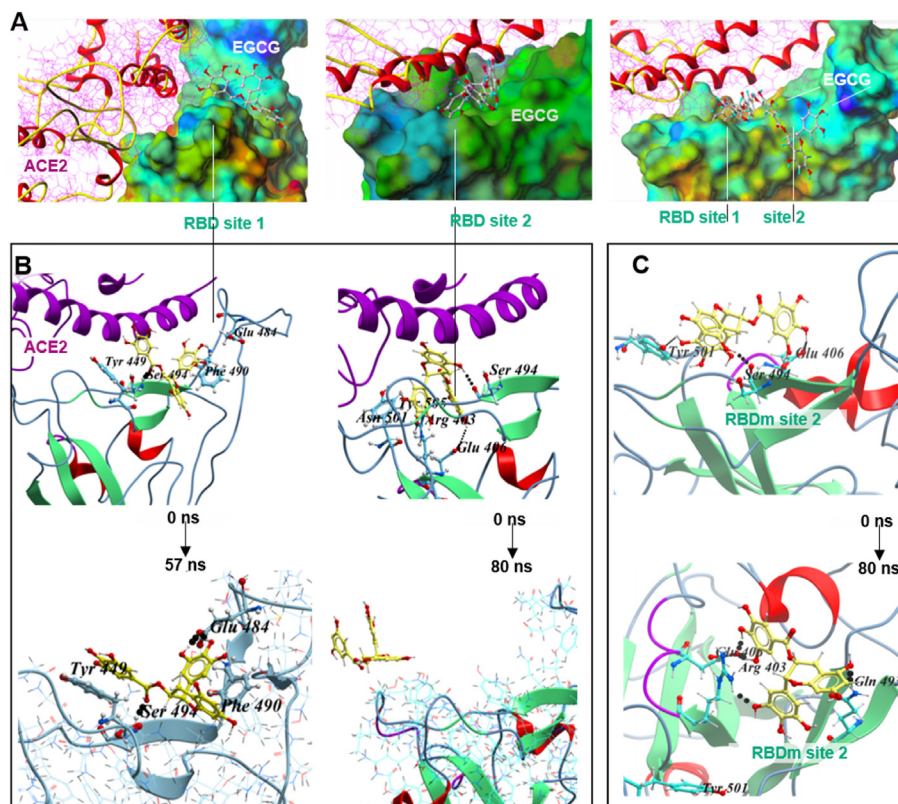
Fig. 3. EGCG complexes with RBD and RBDm. (A) Docking results: EGCG bound to ACE2-opposing sites on RBD surface. RBD surface is colored according to the charge distribution. (B) Molecular dynamics of RBD-EGCG complexes. (C) Molecular dynamics of the RBDm-EGCG complex.

ACE2 interface, Fig. 3A) were optimized and further analyzed using molecular dynamics (MD) simulations. In the case of RBD (Fig. 3B), the EGCG-site 1 complex was stable throughout the simulation. EGCG formed h-bonds with Ser494 and Glu484 (Fig. S2A), as well as stacking contacts with Tyr449 and Phe490 residues (Fig. S2B). Evolution of the stacking interactions was visualized as time plots of the distances between centers of mass of EGCG and Tyr/Phe rings and the angles between the normal to the respective planes. The EGCG-site 2 complex fell apart by 80 ns, despite multiple contacts in the starting conformation (Fig. S2), suggesting transient interactions.

Interestingly, EGCG binding at site 2 turned out to be much more likely in the case of RBDm. EGCG formed multiple h-bonds with RBDm site 2, and the complex was stable throughout the simulation (Fig. S1). Initial binding was driven by hydrophobic interactions. However, the EGCG-induced conformational rearrangement of RBDm enabled energetically favorable electrostatic interactions, including EGCG-Arg403 contacts (Fig. 3C). The contributions of electrostatic and Van der Waals interactions, as well solvation energy, to the binding energy are shown in Fig. S3. Free energy estimations confirmed that EGCG tended to bind RBDm more efficiently that RBD ($\Delta E\_average = -22.1$ kcal/mol for RBDm versus -16.7 and -11.8 kcal/mol for RBD sites 1 and 2, respectively). These results agree with the EGCG-RBD/RBDm binding curves (Fig. 2B).

4. Conclusions

To summarize, we have shown that anti-SARS-CoV-2 activity of EGCG arises mainly from its affinity to the spike viral protein. *In vitro* and *in silico* data indicate that EGCG binds the N501Y spike mutant slightly more efficiently than the original protein and should be considered as a protective agent against infection with "UK Variant" SARS-CoV-2.

Authors' contribution

Conceptualization: M.L., V.L.; methodology: M.L., V.L., D.L., A.I., L.K., V.T., G.P.; investigation: V.T., A.V., A.S., O.L., A.K., T.V., V.M., O.Z., A.E., E.S.; writing (original draft): A.V., A.E., V.T.; writing (critical revision): M.A., V.L., L.K.

Funding

Declaration of competing interest

The authors declare no conflict of interest.

Appendix A. Supplementary data

References

[1] S. Mhatre, T. Srivastava, S. Naik, V. Patravale, Antiviral activity of green tea and black tea polyphenols in prophylaxis and treatment of COVID-19: a review,

Phytomedicine 85 (2021) 153286.

[2] J. Liu, B. Bodnar, F. Meng, A. Khan, X. Wang, et al., Epigallocatechin gallate from green tea effectively blocks infection of SARS-CoV-2 and new variants by inhibiting spike binding to ACE2 receptor, bioRxiv doi, https://doi.org/10.1101/2021.03.17.435637, 2021.

[3] E. Ohgitani, M. Shin-Ya, M. Ichitani, M. Kobayashi, T. Takihara, et al., Significant inactivation of SARS-CoV-2 by a green tea catechin, a catechin-derivative and galloylated theaflavins in vitro, bioRxiv doi, https://doi.org/10.1101/2020.12.04.412098, 2020.

[4] P. Maisonnasse, J. Guedj, V. Contreras, et al., Hydroxychloroquineuse against SARS-CoV-2 infection in non-human primates, Nature 585 (2020) 584–587.

[5] T. Ou, H. Mou, L. Zhang, A. Ojha, H. Choe, M. Farzan, Hydroxychloroquine-mediated inhibition of SARS-CoV-2 entry is attenuated by TMPRSS2, PLoS Pathog. 17 (1) (2021), e1009212.

[6] X. Yao, F. Ye, M. Zhang, C. Cui, B. Huang, et al., In vitro antiviral activity and projection of optimized dosing design of hydroxychloroquine for the treatment of severe acute respiratory syndrome coronavirus 2 (SARS-CoV-2), Clin. Infect. Dis. 71 (2020) 732–739.

[7] S. Mhatre, S. Naik, V. Patravale, A molecular docking study of EGCG and theaflavin digallate with the druggable targets of SARS-CoV-2, Comput. Biol. Med. 129 (2021) 104137.

[8] S. Singh, Sk MdF, A. Sonawane, P. Kar, S. Sadhukhan, Plant-derived natural polyphenols as potential antiviral drugs against SARS-CoV-2 via RNA-dependent RNA polymerase (RdRp) inhibition: an in-silico analysis, J. Biomol. Struct. Dyn. (2020), https://doi.org/10.1080/07391102.2020.1796810.

[9] M. Jang, Y.-I. Park, Y.-E. Cha, R. Park, S. Namkoong, et al., Tea polyphenols EGCG and theaflavin inhibit the activity of SARS-CoV-2 3CL-protease in vitro, Evid. base Compl. Alternative Med. 2020 (2020) 5630838.

[10] J. Park, R. Park, M. Jang, Y.-I. Park, Therapeutic potential of EGCG, a green tea polyphenol, for treatment of coronavirus diseases, Life 11 (3) (2021) 197.

[11] S. Andrade, J.A. Loureiro, M.C. Periera, Green tea extract-biomembrane interaction study: the role of its two major components, (−)-epigallocatechin gallate and (−)-epigallocatechin, Biochim. Biophys. Acta Biomembr. 1863 (2021) 183476.

[12] T.P. Sheahan, A.C. Sims, Sh Zhou, R.L. Graham, A.J. Pruijssers, et al., An orally bioavailable broad-spectrum antiviral inhibits SARS-CoV-2 in human airway epithelial cell cultures and multiple coronaviruses in mice, Sci. Transl. Med. 12 (541) (2020), eabb5883.

[13] S.K. Patra, F. Rizzi, A. Silva, D.O. Rugina, S. Bettuzzi, Molecular targets of (-)-epigallocatechin-3-gallate (EGCG): specificity and interaction with membrane lipid rafts, J. Physiol. Pharmacol. 59 (Suppl 9) (2008) 217–235.

[14] T.N. Starr, A.J. Greaney, S.K. Hilton, D. Ellis, K.H.D. Crawford, A.S. Dingens, M.J. Navarro, J.E. Bowen, M.A. Tortorici, A.C. Walls, N.P. King, D. Veesler, J.D. Bloom, Deep mutational scanning of SARS-CoV-2 receptor binding domain reveals constraints on folding and ACE2 binding, Cell 182 (5) (2020) 1295–1310, e20.

[15] F. Ali, A. Kasry, M. Amin, The new SARS-CoV-2 strain shows a stronger binding affinity to ACE2 due to N501Y mutant, Med. Drug Discov. 10 (2021) 100086.

[16] B. Luan, H. Wang, T. Huynh, Enhanced binding of the N501Y-mutated SARS-CoV-2 spike protein to the human ACE2 receptor: insights from molecular dynamics simulations, FEBS Lett. 595 (2021) 1454–1461.

[17] X. Zhu, Dh Mannar, ShS. Srivastava, A.M. Berezuk, J-Ph Demers, Cryo-electron microscopy structures of the N501Y SARS-CoV-2 spike protein in complex with ACE2 and 2 potent neutralizing antibodies, PLoS Biol. 19 (4) (2021), e3001237.

[18] L. Kozlovskaya, A. Piniaeva, G. Ignatyev, A. Selivanov, A. Shishova, et al., Isolation and phylogenetic analysis of SARS-CoV-2 variants collected in Russia during the COVID-19 outbreak, Int. J. Infect. Dis. 99 (2020) 40–46.

[19] G. Karber, Beitragzurkollecktiven behandlungpharmakologischer reihenversuche, Arch. Exptl. Pathol. Pharmakol. 162 (1931) 480–483.

[20] Møller Chr, M.S. Plesset, Note on an approximation treatment for many-electron systems, Phys. Rev. 46 (7) (1934) 618–622.

[21] V. Barone, M. Cossi, Quantum calculation of molecular energies and energy gradients in solution by a conductor solvent model, J. Phys. Chem. 102 (11) (1998) 1995–2001.

[22] U.C. Singh, P.A. Kollman, An approach to computing electrostatic charges for molecules, J. Comput. Chem. 5 (1984) 129–145.

[23] C.I. Bayly, P. Cieplak, W.D. Cornell, P.A. Kollman, A well-behaved electrostatic potential based method using charge restraints for determining atom-centered charges: the RESP model, J. Phys. Chem. 97 (1993) 10269–10280.